A&A 416, 507–514 (2004)
DOI: 10.1051/0004-6361:20034475

Astronomy & Astrophysics

Minor-axis velocity gradients in disk galaxies⋆,⋆⋆

L. Coccato[1], E. M. Corsini[1], A. Pizzella[1], L. Morelli[1,2], J. G. Funes S. J.[3], and F. Bertola[1]

[1] Dipartimento di Astronomia, Università di Padova, vicolo dell'Osservatorio 2, 35122 Padova, Italy
[2] European Southern Observatory, 3107 Alonso de Cordova, Santiago, Chile
[3] Vatican Observatory, University of Arizona, Tucson, AZ 85721, USA

Received 8 October 2003 / Accepted 25 November 2003

Abstract. We present the ionized-gas kinematics and photometry of a sample of 4 spiral galaxies which are characterized by a zero-velocity plateau along the major axis and a velocity gradient along the minor axis, respectively. By combining these new kinematical data with those available in the literature for the ionized-gas component of the S0s and spirals listed in the Revised Shapley-Ames Catalog of Bright Galaxies we realized that about 50% of unbarred galaxies show a remarkable gas velocity gradient along the optical minor axis. This fraction rises to about 60% if we include unbarred galaxies with an irregular velocity profile along the minor axis. This phenomenon is observed all along the Hubble sequence of disk galaxies, and it is particularly frequent in early-type spirals. Since minor-axis velocity gradients are unexpected if the gas is moving onto circular orbits in a disk coplanar to the stellar one, we conclude that non-circular and off-plane gas motions are not rare in the inner regions of disk galaxies.

Key words. galaxies: kinematics and dynamics – galaxies: elliptical and lenticular, cD – galaxies: spiral – galaxies: structure

1. Introduction

The ionized-gas velocity curves measured along the disk major axis are commonly adopted to derive the mass distribution of spirals within their optical region (see Sofue & Rubin 2001 for a review). In the past decades the central velocity gradient of the gas rotation curves has been used to constrain the amount and distribution of the visible component in high surface brightness galaxies (e.g. Kent 1986; Persic et al. 1996). During recent years a lively debate concerning the dark matter distribution in the central regions of low surface brightness galaxies has been triggered by the measurement of the inner slope of the ionized-gas rotation curves in a large sample of these galaxies (McGaugh et al. 2001; de Block et al. 2001).

These mass models are based on the hypothesis that ionized gas in central regions is moving onto circular orbits and in the plane of the stellar disk. However, evidence has mounted that the kinematic behavior of the gaseous component in inner regions of disk galaxies is more complex. Indeed ionized gas can have an intrinsic velocity dispersion and its velocity can be lower than the circular speed derived from dynamical models based on the stellar kinematics and photometry (Fillmore et al. 1986; Bertola et al. 1995; Cinzano et al. 1999), a large number of kinematically-decoupled gaseous components rotating in a different plane with respect to that of the stellar disk have been found in early-type disk galaxies (Bertola et al. 1992; Bertola & Corsini 2000; Corsini et al. 2003), and non-circular gas motions have been observed in triaxial bulges (Bertola et al. 1989; Gerhard et al. 1989; Berman 2001). Moreover the vast majority of the gas velocity fields measured by Hubble Space Telescope in the nuclei of nearby spiral galaxies are not regular and possibly affected by non-gravitational forces (Sarzi 2003). This poses new questions about the reliability of gas kinematics to derive the mass density profile in the central regions of galaxies.

The presence of a velocity gradient along the disk minor axis is the kinematic signature that ionized gas is not moving onto circular orbits in a disk which is coplanar to that of the stars. To point out that this is a common phenomenon we have built a compilation of the minor-axis velocity profiles available from long-slit spectroscopy for the disk galaxies listed in the Revised Shapley-Ames Catalog of Bright Galaxies (Sandage & Tammann 1981, RSA hereafter). In addition, we have obtained the minor-axis velocity profiles for 4 spiral galaxies, whose major-axis kinematics are characterized by a remarkable

Send offprint requests to: L. Coccato,
e-mail: coccato@pd.astro.it

⋆ Based on observations carried out at the European Southern Observatory in La Silla (Chile) (ESO 69.B-0706 and 70.B-0338), with the Multiple Mirror Telescope which is a joint facility of the Smithsonian Institution and the University of Arizona, and with the Italian Telescopio Nazionale Galileo (AOT-5, 3-18) at the Observatorio del Roque de los Muchachos in La Palma (Spain).

⋆⋆ Table 1 is only available in electronic form at http://www.edpsciences.org. Table 5 is only available in electronic form at the CDS via anonymous ftp to cdsarc.u-strasbg.fr (130.79.128.5) or via http://cdsweb.u-strasbg.fr/cgi-bin/qcat?J/A+A/416/507

zero-velocity plateau. All these galaxies show a gas velocity gradient along the disk minor axis. Such a peculiar kinematics may be also the signature of an inner polar disk as those we have recently found in early-type spiral galaxies (Corsini et al. 2003).

This paper is organized as follows. The list of the RSA disk galaxies for which the ionized-gas velocity profile has been measured along the disk minor axis is given in Sect. 2. The spectroscopic observations and data analysis of our 4 sample galaxies are described in Sect. 3. The resulting ionized-gas kinematics are discussed in Sect. 4. Our conclusions are presented in Sect. 5.

2. Minor-axis velocity profiles of ionized gas of the disk galaxies in the Revised Shapley-Ames Catalog

To get an exhaustive picture of the phenomena related to non-circular and off-plane motions of ionized gas in disk galaxies, we compiled in Table 1 both data from the literature and from the present paper. In Table 1 we listed all the disk galaxies of RSA for which the ionized-gas velocity profiles has been measured along the minor axis by means of long-slit spectroscopy. The table gives the main properties of the galaxies, namely the morphological classification, size, inclination, major-axis position angle, apparent magnitude and recession velocity. The position angle of the observed major and minor axis as well as the related bibliographic reference are reported in Table 1 too.

Minor-axis velocity data have been found in literature for 138 out of 1101 disk galaxies (12%), whose RSA morphological type ranges from S0 to Sm, including barred systems. During this process we realized that the velocity curves of the ionized-gas component have a variety of shapes. For purpose of classification we assigned the minor-axis velocity profiles to five different classes, which we named Z, O, C, G, and I, as follows:

- Z: a zero velocity gradient is observed for the ionized-gas component along the minor axis;
- O: an overall gas velocity profile is observed along the minor axis without zero-velocity points out to the last measured radius;
- C: non-zero gas velocities are measured only in the central regions along the minor axis. The gas velocity profile shows a steep gradient rising to a maximum observed velocity of few tens of km s^{-1} in the inner few arcsec, then the velocity drops to zero at larger radii;
- G: a central velocity gradient is observed, but the limited radial extension of the data does not allow us to distinguish between overall or centrally-confined non-zero velocities;
- I: there is evidence of non-zero velocities along the minor axis but the velocity is either too poorly detected or too asymmetric to be assigned to the previous classes.

In Fig. 1 we show a prototypic example for each class of minor-axis velocity profile. The classification of the minor-axis velocity profiles of RSA galaxies is given in Table 1.

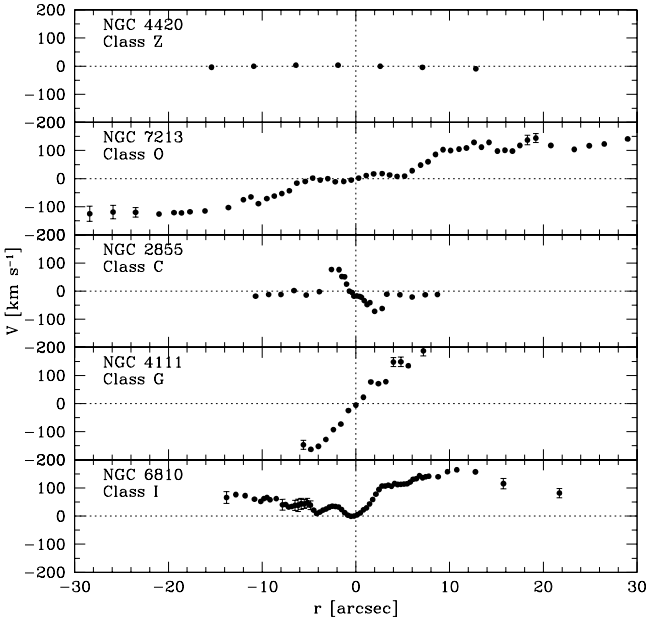

Fig. 1. The ionized-gas velocity profiles measured along the optical minor axis of NGC 4420 (PA = 98°, Fisher et al. 1997), NGC 7213 (PA = 34°, Corsini et al. 2003), NGC 2855 (PA = 30°, Corsini et al. 2002), NGC 4111 (PA = 60°, Fisher 1997), and NGC 6810 (PA = 86°, this paper) are given as prototypical examples for the five classes of minor-axis velocity profiles described in Sect. 2. Errorbars smaller than symbols are not plotted.

3. Sample, observations and data reduction

NGC 949, NGC 2460, NGC 2541, and NGC 6810 are unbarred spiral galaxies which belong to a sample of 16 bright ($B_T \leq 13.5$) and nearby ($V_\odot \leq 3500$ km s^{-1}) spirals studied by Coccato et al. (2004) to search for a circumnuclear Keplerian disk (Bertola et al. 1998; Funes et al. 2002). The main properties of the sample galaxies are summarized in Table 2. The major-axis rotation curve of their gaseous component is characterized by a remarkable zero-velocity plateau. We decided to obtain spectra along their minor axis to investigate the possible presence of a velocity gradient. The position angles of the major and minor axis were chosen according to de Vaucouleurs et al. (1991, RC3 hereafter) and therefore relate to the orientation of the outermost isophotes. This is confirmed by the isophotal analysis of the images available for the sample galaxies in the NASA/IPAC Infrared Science Archive of the Two Micron All Sky Survey (2MASS) and in the archive by Frei et al. (1996).

3.1. Kinematic data

The long-slit spectroscopic observations of the sample galaxies were carried out at the Roque de los Muchachos Observatory in La Palma with the Telescopio Nazionale Galileo (TNG), at the European Southern Observatory in La Silla with the New Technology Telescope (NTT), and at the Multiple Mirror Telescope Observatory in Arizona with the Multiple Mirror Telescope (MMT) in 2002. The details about the instrumental setup of each observing run as well as the value of the seeing

Table 2. Parameters of the sample galaxies.

Object	Morp. type		B_T	PA	i	$V_\odot$	D	Scale	$M^0_{B_T}$
[name]	[RSA]	[RC3]	[mag]	[°]	[°]	[km s^{-1}]	[Mpc]	[pc/″]	[mag]
(1)	(2)	(3)	(4)	(5)	(6)	(7)	(8)	(9)	(10)
NGC 0949	Sc(s)III	Sb(rs):?	12.40	145	58	608 ± 10	11.2	54.5	−18.47
NGC 2460	Sab(s)	Sa(s)	12.72	40	42	1452 ± 10	21.3	103.0	−19.35
NGC 2541	Sc(s)III	Scd(s)	12.26	165	60	540 ± 10	8.3	40.5	−18.03
NGC 6810	Sb	Sab(s):sp	12.37	176	78	1961 ± 5	24.3	117.8	−20.44

NOTES – Column (2): morphological classification from RSA. Column (3): morphological classification from RC3. Column (4): apparent total blue magnitude from RC3. Column (5): major-axis position angle from RC3. Column (6): inclination derived as $\cos^2 i = (q^2 - q_0^2)/(1 - q_0^2)$. The observed axial ratio q is taken from RC3 and the intrinsic flattening has been assumed following Guthrie (1992) with RC3 morphological classification. Column (7): heliocentric velocity of the galaxy derived as center of symmetry of the rotation curve of the gas with eliocentric correction. Column (8): distance obtained as V_0/H_0 with $H_0 = 75$ km s^{-1} Mpc^{-1} and V_0 the systemic velocity derived from $V_\odot$ corrected for the motion of the Sun with respect of the Local Group as done in the RSA. Column (10): absolute total blue magnitude corrected for inclination and extinction from RC3.

Table 3. Setup of the spectroscopic observations.

Parameter	Run 1	Run 2	Run 3	Run 4
Date	Jan 19–21, 2002	May 16, 2002	Oct 08, 2002	Oct 31–Nov 01, 2002
Instrument	TNG+DOLORES	NTT+EMMI	NTT+EMMI	MMT+Blue Channel
Grating/Grism	VPH #9 1435 gr mm^{-1}	#6 1200 gr mm^{-1}	#7 600 gr mm^{-1}	1200 gr mm^{-1}
CCD	2048 × 2048 Loral	#36 2048 × 2048 Tek	2048 × 4096 MIT/LL	#22 3072 × 1024 Loral
Pixel size	15 × 15 μm^2	24 × 24 μm^2	15 × 15 μm^2	15 × 15 μm^2
Scale	0.″275 pixel^{-1}	0.″32 pixel^{-1}	0.″332 pixel^{-1}	0.″30 pixel^{-1}
Dispersion	0.34 Å pixel^{-1}	0.32 Å pixel^{-1}	0.83 Å pixel^{-1}	0.49 Å pixel^{-1}
Slit width	1.″0	1.″0	1.″0	1.″5
Wavelength range	6210–6870 Å	6400–7020 Å	5630–6970 Å	4455–5945 Å
Instrumental *FWHM*	1.63 Å	1.12 Å	2.34 Å	2.02 Å
Instrumental σ^a	32 km s^{-1}	22 km s^{-1}	45 km s^{-1}	53 km s^{-1}
Seeing *FWHM*	1.″5–2.″0	1.″8	1.″3	1.″8–2.″2

[a] At Hα in Run 1–3, and at Hβ in Run 4.

FWHM as measured by fitting a two-dimensional Gaussian to the guide star are given in Table 3.

Medium-resolution spectra were taken along both the major and minor axis after centering the galaxy nucleus on the slit using the guiding camera. A comparison spectrum was taken before and/or after every object exposure. The typical integration time of the galaxy spectra were 1800 s and 2700 s. Total integration times and slit position angles of the galaxy spectra as well as the log of observations are given in Table 4.

Basic data reduction was performed as in Corsini et al. (1999). Using standard `ESO-MIDAS`[1] routines, all the spectra were bias subtracted, flat-field corrected by quartz lamp and twilight exposures, cleaned from cosmic rays, and wavelength calibrated. The flat-field correction was performed by means of both quartz lamp and twilight sky spectra in order to correct for pixel-to-pixel sensitivity variations and large-scale illumination patterns due to slit vignetting. Cosmic rays were identified by comparing the photon counts in each pixel with the local mean and standard deviation and they were eliminated by interpolating over. Residual cosmic rays were eliminated by manually editing the spectra. We checked that the wavelength rebinning was done properly by measuring the difference between the measured and predicted wavelengths (Osterbrock et al. 1996) for the brightest night-sky emission lines in the observed spectral ranges. The resulting accuracy in the wavelength calibration is typically of 5 km s^{-1}. Instrumental resolution was derived as the mean of Gaussian *FWHM*'s measured

Table 4. Log of the spectroscopic observations.

Object	Run	PA [°]	Axis	Exp. time [s]
NGC 949	4	55	Minor	2 × 2700
NGC 949	1	145	Major	2 × 2700
NGC 2460	4	130	Minor	2 × 2700
NGC 2460	1	40	Major	2 × 2700
NGC 2541	4	75	Minor	2 × 2700
NGC 2541	1	165	Major	1 × 2700
NGC 6810	3	86	Minor	1 × 1800
NGC 6810	2	176	Major	1 × 2400

[1] `MIDAS` is developed and maintained by the European Southern Observatory.

for a number of unblended arc-lamp lines of a wavelength calibrated spectrum. The mean *FWHM* of the arc-lamp lines and the corresponding resolution at Hα (Run 1–3) and Hβ (Run 4) are given in Table 3. After the calibration all the spectra were corrected for CCD misalignment. The contribution of the sky was determined from the outermost $\sim$10″ at the two edges of the resulting frames where the galaxy light was negligible, and then subtracted. The spectra obtained for a given galaxy along the same position angle were coadded using the center of the stellar-continuum radial profile as reference.

The ionized-gas kinematics was measured by the simultaneous Gaussian fit of the emission lines present in the spectra (namely [N II] $\lambda\lambda$6548, 6583, Hα, and [S II] $\lambda\lambda$6716, 6731 in Run 1–3, Hβ and [O III] $\lambda\lambda$4959, 5007 in Run 4). The galaxy continuum was removed row-by-row by fitting a fourth to sixth order polynomial avoiding all the spectral regions with strong emission and absorption features. We fitted in each row of the continuum-subtracted spectrum a Gaussian to each emission line, assuming them to have the same line-of-sight velocity and velocity dispersion (corrected for heliocentric velocity and instrumental *FWHM*, respectively). In the spectra an additional absorption Gaussian has been added in the fit to take into account for the presence of the Hα or Hβ absorption line and the flux ratio of the [N II] $\lambda\lambda$6548, 6583 lines have been fixed to 1:3. Far from the galaxy center (for $|r| \gtrsim 10''$) we averaged adjacent spectral rows in order to increase the signal-to-noise ratio of the relevant emission lines. Errors on the gas velocity and velocity dispersion were derived from photon statistics and CCD readout noise by means of Monte Carlo simulations.

The line-of-sight velocity and velocity dispersion profiles we measured for the gaseous component along the major and minor axis of the sample galaxies are presented in Fig. 2 and values are reported in Table 5. The line-of-sight velocities of the ionized-gas are the observed ones after subtracting the systemic velocities of Table 2 and without applying any correction for galaxy inclination.

3.2. Photometric data

We retrieved the 2MASS *H* band images of NGC 949 (3.′5 × 3.′5), NGC 2460 (3.′0 × 3.′0), NGC 2541 (13.′3 × 13.′3) and NGC 6810 (5.′0 × 5.′0) from the NASA/IPAC Infrared Science Archive. The galaxy images were reduced and flux calibrated with the standard 2MASS extended source processor GALWORKS (Jarrett et al. 2000). Images have a spatial resolution of 1″ and were obtained with a typical seeing *FWHM* $\sim$ 1″.

The signal-to-noise of the 2MASS image of NGC 2541 was too low to perform a reliable photometric analysis, we therefore retrieved the *i* band image (4.′0 × 4.′0) obtained by Frei et al. (1996) too. They already performed all the basic steps of data reduction, including bias subtraction, flat-fielding, cleaning of cosmic rays, and subtraction of sky background and stellar sources.

We analyzed the isophotal profiles of the background and star subtracted images by masking the residual foreground stars, and then fitting ellipses to the isophotes with the IRAF[2] task ELLIPSE. We first allowed the centers of the ellipses to vary, to test whether the galaxies were disturbed. Within the errors of the fits, we found no evidence of a varying center. The ellipse fits were therefore repeated with the ellipse centers fixed. The resulting azimuthally averaged surface brightness, ellipticity, and position angle profiles for the sample galaxies are plotted in Fig. 3.

4. Ionized-gas kinematics and near-infrared photometry

The following kinematic photometric features are noteworthy in the sample galaxies.

The central velocity gradient along the major axis is zero (NGC 949, NGC 2541, NGC 6810) or at least less steep (NGC 2460) than that we measured for radii larger than $\approx$3″. Further out the gas velocity increases to reach a maximum and then remains constant out to the last observed radius. Non-zero gas velocities are measured along the minor axis of all the sample galaxies, in spite of which would be expected if the gas traced the circular velocity in the disk plane. The gas velocity dispersion remains low ($\lesssim$50 km s^{-1}) except for few radii along the major axis of NGC 2460 and in the inner regions of NGC 6810 where it reaches $\approx$120 km s^{-1}. Qualitatively all these data indicate that the gas is predominantly supported by rotation, and exclude the presence of a dynamically hot gas as found in some bulges (Bertola et al. 1995; Cinzano et al. 1999). We attribute the minor-axis velocity gradients to the presence of kinematically-decoupled component which is not rotating in the plane of the stellar disk. The reversal of the gas velocities measured along the minor axis of NGC 949 and NGC 2460, and the receding velocities observed along the minor axis of NGC 6810 are suggestive of an even more complex gas structure involving a warp and an outflow, respectively.

We observed a large isophotal twist in the inner $\sim$10″ of the sample galaxies which is associated with an increase of ellipticity at small radii. These photometric features can be interpreted as the signature of bulge triaxiality (e.g. Bertola et al. 1991). The bump observed at $\sim$20″ in the surface-brightness profiles of NGC 949 and NGC 6810 suggests the presence of a bar. There is no signature of a bar in the photometric profiles of NGC 2450 and NGC 2541. For radii larger than $\sim$20″ the position angle and ellipticity settle to almost constant values as expected when the disk component dominates the galaxy light. The values of position angle and ellipticity we measured at the farthest observed radius are consistent within the errors with those in *B* band listed in RC3, apart from the ellipticity of NGC 6810. We attribute the different shape of the outer isophotes of NGC 6810 to the dust lanes crossing the disk (see Panel 145, Sandage & Bedke 1994). For all the sample galaxies the slit position in spectroscopic observations corresponds to the major and minor axis of the disk.

[2] IRAF is distributed by NOAO, which is operated by AURA Inc., under contract with the National Science Foundation.

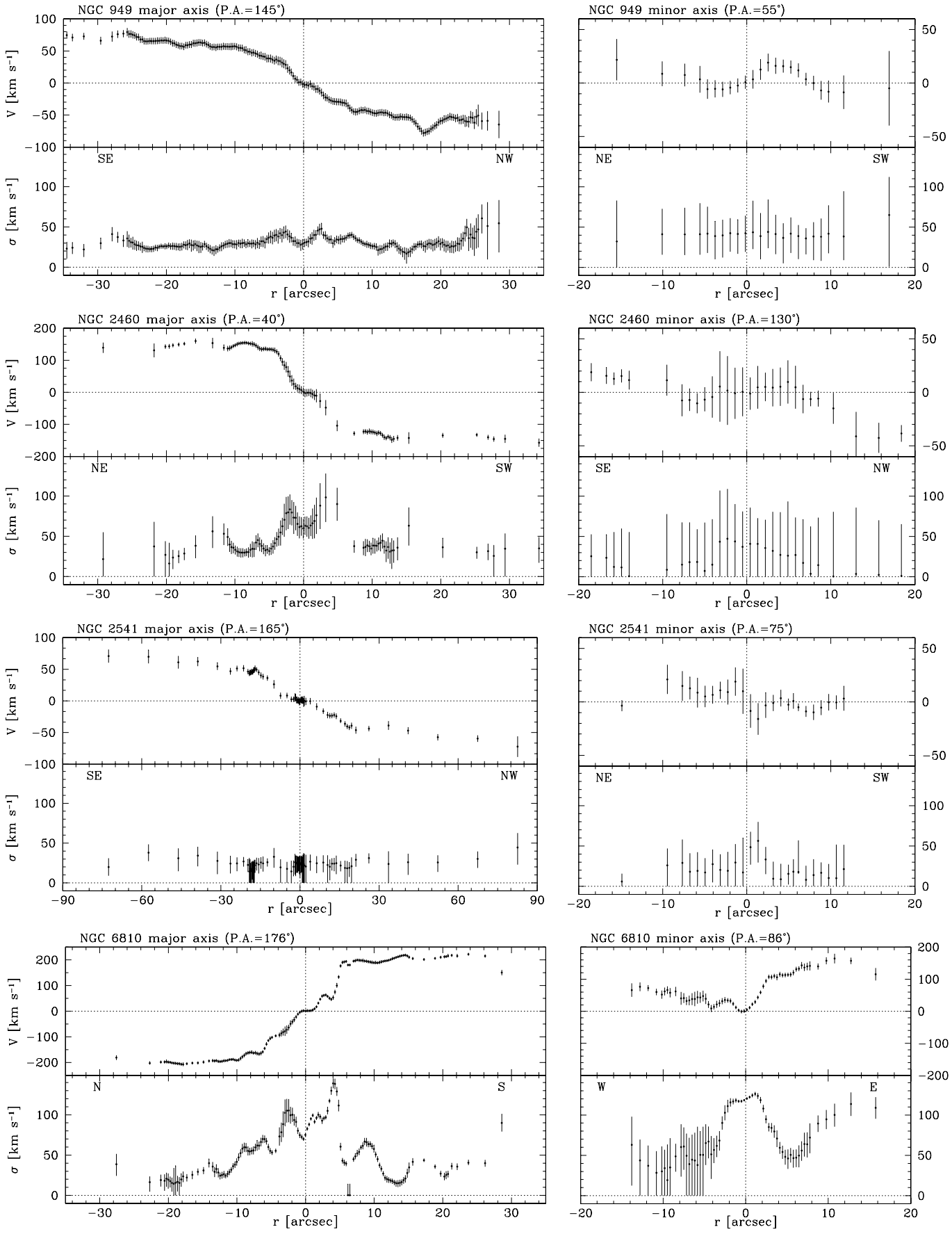

Fig. 2. Ionized-gas kinematics measured along the optical major (*left panels*) and minor axes (*right panels*) of the 4 sample galaxies. Errorbars smaller than symbols are not plotted.

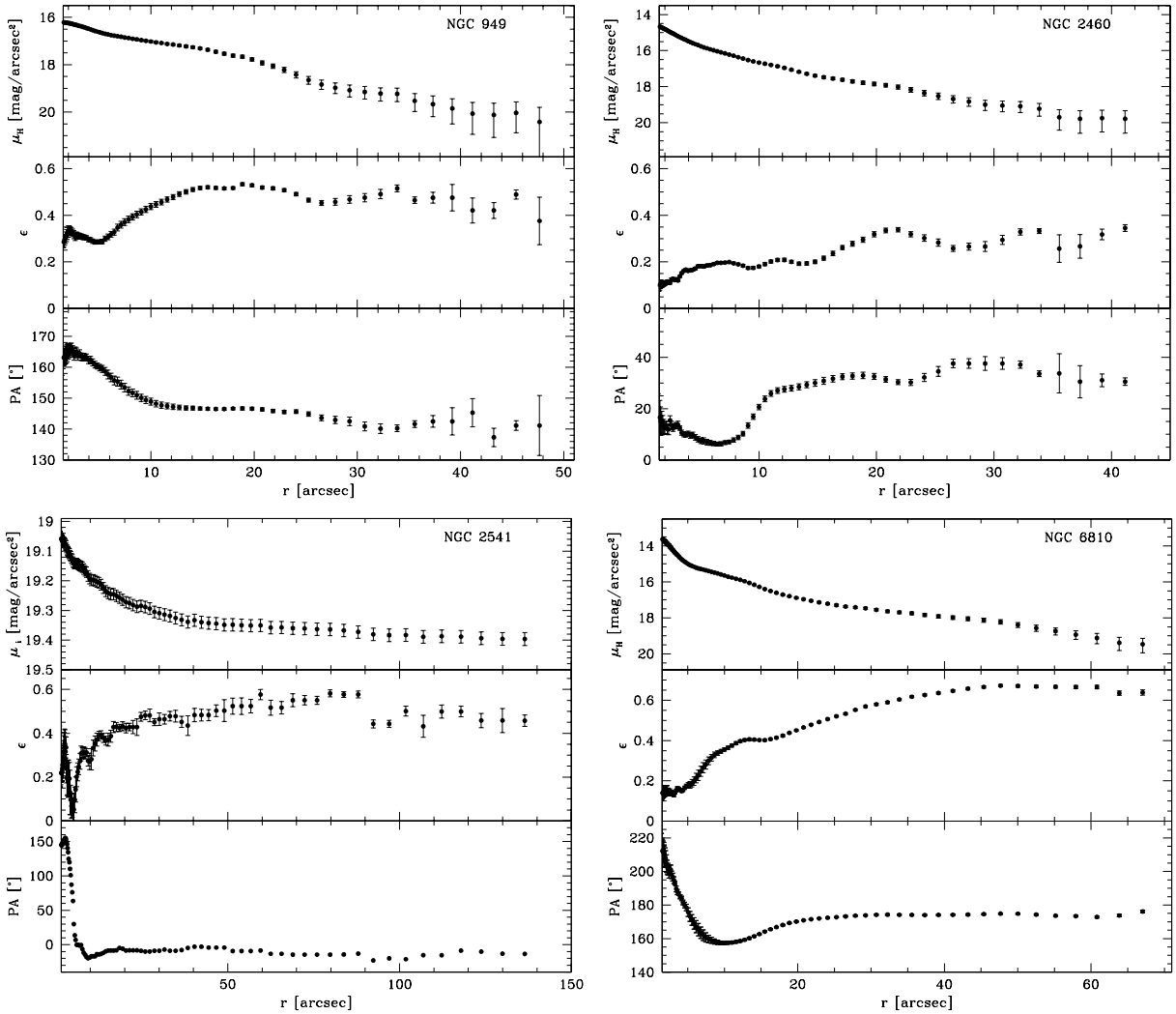

Fig. 3. Surface-brightness (*upper panel*), ellipticity (*central panel*) and position angle (*lower panel*) radial profiles for the sample galaxies. Data for NGC 949, NGC 2460, and NGC 6810 and in *H* band, data for NGC 2541 are in *i* band.

5. Discussion and conclusions

By combining the new kinematic data of our sample galaxies with those available in the literature for the RSA galaxies we have the minor-axis velocity profiles of the ionized-gas component for a sample of 142 disk galaxies. In Fig. 4 we show the distribution of the gas velocity gradients measured along the optical minor axis these galaxies according to their RSA morphological classification. Although the effective frequency of the presence gas velocity gradients along the minor axis of bright disk galaxies can be properly addressed only with the analysis of a magnitude limited sample, Fig. 4 favors a picture in which this is a widespread phenomenon which is not limited to few peculiar objects: 95/142 (67%) of the studied galaxies shows motions (including irregular ones) along the minor axis.

The presence of a minor-axis velocity gradient in 16/25 (64%) of the available barred galaxies is explained as due to the non-circular (e.g. Athanassoula 1992) and off-plane (e.g. Friedli & Benz 1993) motions induced on the gaseous component by the tumbling triaxial potential of the bar.

We find that 54/117 (46%) of the unbarred galaxies shows a minor-axis gas velocity gradient and the phenomenon is particularly frequent in the earliest morphological types. If we consider also the unbarred galaxies with an irregular velocity profile along the minor axis, the fraction rises to 75/117 (64%). Most of these velocity gradients has to be attributed to the presence of non-detected bars since ≈40% of the spiral galaxies without a strong optical bar reveal a strong bar when observed in near infrared (Eskridge et al. 2000). However, it must be noted that in addition to the presence of a bar other mechanisms can be invoked to explain the observed velocity gradients.

A large fraction of the S0 galaxies (6/16, 38%) listed in Table 1 is characterized by an overall gas velocity profile along the optical minor axis. If the gas in all S0 galaxies is of external origin (Bertola et al. 1992; Kuijken et al. 1996) then the observed kinematics can be straightforwardly interpreted as due to accreted gas which is rotating in a warped/inclined disk with respect to the stellar disk (e.g. NGC 4753, Steinman-Cameron et al. 1992). This is a stable configuration in a barred potential when gas is settled onto the so-called anomalous orbits (e.g. NGC 128, Emsellem & Arsenault 1996).

The presence of non-zero velocities confined in the nuclear regions along the minor axis is particularly frequent in

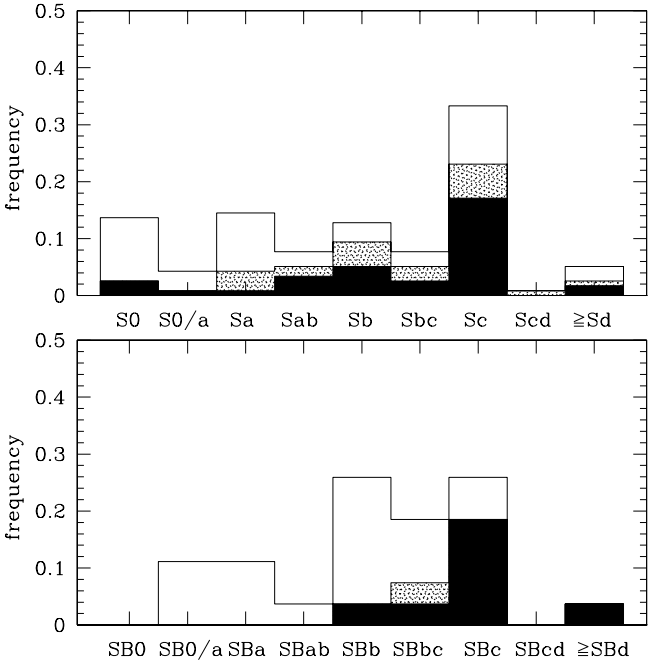

Fig. 4. Distribution of the gas velocity gradient along the optical minor axis of the unbarred (*upper panel*) and barred (*lower panel*) galaxies we collected in Table 1 according to their RSA morphological classification. The white and black regions identify galaxies with (Classes O, C, and G) and without a minor-axis velocity gradient (Class Z), respectively. The shaded region identify galaxies assigned to Class I. The last bins of the panels include all the galaxies with a morphological type later than Sd and SBd, respectively.

bulge-dominated spirals. Since there is no significant trend in the bar fraction as a function of morphology in either the optical or near infrared photometry (Eskridge et al. 2000), this finding suggests that at least some of the minor-axis velocity gradients are closely related to bulge prominence. Indeed the intrinsic shape of bulges is triaxial (Bertola et al. 1991) and two equilibrium planes are allowed for the gaseous component. We are left with two alternative scenarios as viable mechanisms to explain minor-axis velocity gradients in early-type spirals. All the gaseous component lies on the principal plane perpendicular to the bulge short axis and moves onto closed elliptical orbits, which become nearly circular at large radii (de Zeeuw & Franx 1989; Gerhard et al. 1989; Corsini et al. 2003). A central velocity gradient is measured along both the major and minor axis as due to the orientation of the inner elliptical orbits lying on the disk plane and seen at an intermediate angle between their intrinsic major and minor axes. The minor-axis gas velocity profile drops to zero where elliptical orbits become circular. Alternatively, only the outer gaseous component lies on the plane perpendicular to the short axis of bulge, while the inner gas is rotating in the principal plane perpendicular to the long axis of the bulge giving rise to an inner polar disk (Corsini et al. 2003). If this is the case the central velocity gradient observed along the disk minor axis is associated with a central zero-velocity plateau (or at least to a shallower velocity gradient) along the disk major axis.

Acknowledgements. We thank the referee, O. Sil'chenko, for the suggestions which helped us to improve the paper. We are also grateful to J. A. L. Aguerri for useful discussions. This research has made use of the NASA/IPAC Infrared Science Archive, which is operated by the Jet Propulsion Laboratory, California Institute of Technology, under contract with the National Aeronautics and Space Administration.

References

Afanasyev, V. L., Burenkov, A. N., Zasov, A. V., & Silchenko, O. K. 1992, AZh, 69, 19
Aguero, E. L., & Paolantonio, S. 1997, AJ, 114, 102
Athanassoula, E. 1992, MNRAS, 259, 345
Beauvais, C., & Bothun, G. 2001, ApJS, 136, 41
Berman, S. 2001, A&A, 371, 476
Bertola, F., & Corsini, E. M. 1999, in Galaxy Interactions at Low and High Redshift, ed. J. Barnes, & D. B. Sanders (Dordrecht: Kluwer Academic Press), IAU Symp., 186, 149
Bertola, F., Rubin, V. C., & Zeilinger, W. W. 1989, ApJ, 345, L29
Bertola, F., Vietri, M., & Zeilinger, W. W. 1991, ApJ, 374, L13
Bertola, F., Buson, L. M., & Zeilinger, W. W. 1992a, ApJ, 401, L79
Bertola, F., Galletta, G., & Zeilinger, W. W. 1992b, A&A, 254, 89
Bertola, F., Cinzano, P., Corsini, E. M., Rix, H., & Zeilinger, W. W. 1995, ApJ, 448, L13
Bertola, F., Cappellari, M., Funes, J. G., et al. 1998, ApJ, 509, L93
Bettoni, D., & Galletta, G. 1997, A&AS, 124, 61
Bettoni, D., Fasano, G., & Galletta, G. 1990, AJ, 99, 1789
Blackman, C. P. 1980a, MNRAS, 190, 459
Blackman, C. P. 1980b, MNRAS, 191, 123
Blackman, C. P., Wilson, A. S., & Ward, M. J. 1983, MNRS, 202, 1001
Burbidge, E. M., Burbidge, G. R., & Prendergast, K. H. 1960, ApJ, 132, 654
Burbidge, E. M., Burbidge, G. R., & Prendergast, K. H. 1962, ApJ, 136, 339
Burbidge, E. M., Burbidge, G. R., & Prendergast, K. H. 1963, ApJ, 137, 376
Buta, R. 1987, ApJS, 64, 383
Caldwell, N. 1984, ApJ, 278, 96
Caon, N., Macchetto, D., & Pastorizia, M. 2000, ApJS, 127, 39
Carozzi-Meyssonnier, N. 1979, A&AS, 37, 529
Chincarini, G., & Walker, M. F. 1976, ApJ, 149, 487
Chromey, F. R. 1974, A&A, 31, 165
Cinzano, P., Rix, H.-W., Sarzi, M., et al. 1999, MNRAS, 307, 433
Coccato, L., Corsini, E. M., Pizzella, A., & Bertola, F. 2004, in preparation
Comte, G., Monnet, G., & Rosado, M. 1979, A&A, 72, 73
Corsini, E. M., & Bertola, F. 1998, JKPS, 33, 574
Corsini, E. M., Pizzella, A., & Bertola, F. 2002, A&A, 382, 488
Corsini, E. M., Pizzella, A., Coccato, L., & Bertola, F. 2003, A&A, 408, 873
Corsini, E. M., Pizzella, A., Sarzi, M., et al. 1999, A&A, 342, 671
Corsini, E. M., Pizzella, A., Sarzi, M., et al. 2000, in Dynamics of Galaxies: from the Early Universe to the Present, ed. F. Combes, G. A. Mamon & V. Charmandaris (ASP: San Francisco), ASP Conf. Ser., 197, 251
Danziger, I. J., Goss, W. M., & Wellington, K. J. 1981, MNRAS, 195, 33
de Blok, W. J. G., McGaugh, S. S., & Rubin, V. C. 2001, AJ, 122, 2396
Dehnen, W. 1993, MNRAS, 265, 250
Demoulin, M. 1969, ApJ, 157, 69

de Vaucouleurs, D., de Vaucouleurs, A., Corwin, H. G., Jr., et al. 1991, Third Reference Catalog of Bright Galaxies (New York: Springer-Verlag)
de Zeeuw, P. T. & Carollo, C. M. 1996, MNRAS, 281, 1333
de Zeeuw, T., & Franx, M. 1989, ApJ, 343, 617
Duval, M. F. 1981, A&A, 98, 352
Emsellem, E., & Arsenault, R. 1997, A&A, 318, L39
Fillmore, J. A., Boroson, T. A., & Dressler, A. 1986, ApJ, 302, 208
Fisher, D. 1997, AJ, 113, 950
Fisher, D., Illingworth, G., & Franx, M. 1994, AJ, 107, 160
Frei, Z., Guhathakurta, P., Gunn, J. E., & Tyson, J. A. 1996, AJ, 111, 174
Fridman, A. M., Khoruzhii, O. V., Lyakhovich, V. V., et al. 2001, A&A, 371, 538
Friedli, D., & Benz, W. 1993, A&A, 268, 65
Funes, J. G., S. J, Corsini, E. M., Cappellari, M., et al. 2002, A&A, 388, 50
Gerhard, O. E., & Vietri, M. 1986, MNRAS, 223, 377
Goad, J. W. 1974, ApJ, 192, 311
Haynes, M. P., Jore, K. P., Barrett, E. A., Broeils, A. H., & Murray, B. M. 2000, AJ, 120, 703
Higdon, J. L., Buta, R. J., & Purcell, G. B. 1980, AJ, 115, 80
Hunter, D. A., Rubin, V. C., Swaters, R. A., Sparke, L. S., & Levine, S. E. 2002, ApJ, 580, 194
Jarrett, T. H., Chester, T., Cutri, R., et al. 2000, AJ, 119, 2498
Jimenez, R., Verde, L., & Oh, S. P. 2003, MNRAS, 339, 243
Jogee, S., Kenney, J. D. P., & Smith, B. J. 1999, ApJ, 526, 665
Jore, K. P., Broelis, A. H., & Haynes, M. P. 1996, AJ, 112, 438
Kenney, J. D. P., Koopmann, R. A., Rubin, V. C., & Young, J. S. 1996, AJ, 111, 152
Kent, S. M. 1986, AJ, 91, 1301
Keppel, J. W., Dettmar, R. J., Gallagher, J. S., III, & Roberts, M. S. 1991, ApJ, 374, 507
Kuijken, K., Fisher, D., & Merrifield, M. R. 1996, MNRAS, 283, 543
Kuno, N., Tosaki, T., Nakai, N., & Nishiyama, K. 1997, PASJ, 49, 275
Kyazumov, G. A. 1980, SvA, 6, L398
Lake, G, & Dressler, A. 1986, ApJ, 310, 605
Lindblad, P. O., Hjelm, M., Hoegbom, J., et al. 1996, A&AS, 120, 403
Márquez, I., & Moles, M. 1996, A&A, 120, 1
Márquez, I., Boisson, C., Durret, F., & Petitjean, P. 1998, A&A, 333, 459
Márquez, I., Masegosa, J., Moles, M., et al. 2002, A&A, 393, 389
McGaugh, S. S., Rubin, V. C., & de Blok, W. J. G. 2001, AJ, 122, 2381
Moellenhoff, C. 1982, A&A, 108, 130
Moore, B. 1994, Nature, 370, 629
Mulder, P. S., & van Driel, W. 1996, A&A, 309, 403
Munoz Tunon, C., Beckman, J., & Prieto, M. 1987, Rev. Mex. Astron. Astrofis., 14, 144
Osterbrock, D. E., Fulbright, J. P., Martel, A. R., et al. 1996, PASP, 108, 277
Pellet, A. 1976, A&A, 50, 421
Pérez, E., Márquez, I., Marrero, I., et al. 2000, A&A. 353, 893
Persic, M., Salucci, P., & Stel, F. 1996, MNRAS, 281, 27
Peterson, C. J. 1980, PASP 92, 397
Peterson, C. J., & Huntley, J. M. 1980, ApJ, 242, 913
Peterson, C. J., Roberts, M. S., Rubin, V. C., & Ford, W. K., Jr. 1978, ApJ, 226, 770
Pizzella, A., Corsini, E. M., Morelli, L., et al. 2002, ApJ, 573, 131
Prada, F., Gutierrez, C. M., & McKeith, C. D. 1998, ApJ, 495, 765
Reshetnikov, V. P., & Combes, F. 1994, A&A, 291, 57
Rubin, V. C., Burbidge, E. M., Burbidge, G. R., & Prendergast, K. H. 1964, ApJ, 140, 80
Rubin, V. C. 1980, ApJ, 238, 808
Rubin, V. C. 1994a, AJ, 107, 173
Rubin, V. C. 1994b, AJ, 108, 456
Rubin, V. C., & Ford, W. K., Jr. 1970, ApJ, 159, 379
Rubin, V. C., Burbidge, E. M., Burbidge, G. R., & Prendergast, K. H. 1965, ApJ, 141, 885
Rubin, V. C., Thonnard, N., & Ford, W. K., Jr. 1977, ApJ, 217, L1
Rubin, V. C., Roberts, M. S., & Ford, W. K., Jr. 1979, ApJ, 230, 35
Rubin, V. C., Thonnard, N., & Ford, W. K., Jr. 1980, ApJ, 238, 471
Rubin, V. C., Waterman, A. H., & Kenney, J. D. P. 1999, AJ, 118, 236
Ryder, S. D., Zasov, A. V., Sil'Chenko, O. K., McIntyre, V. J., & Walsh, W. 1998, MNRAS, 293, 411
Sandage, A. & Tammann, G. A. 1981, A Revised Shapley-Ames Catalog of Bright Galaxies (Washington D.C.: Carnegie Institution of Washington)
Sandqvist, A., Elfhag, T., & Lindblad, P. O. 1989, A&A, 218, 39
Sakka, K., Oka, S., & Wakamatsu, K. 1973, PASJ, 25, 317
Sarzi, M. 2003, in Coevolution of Black Holes and Galaxies, ed. L. C. Ho (Cambridge: Cambdrige Univ. Press), in press
Sarzi, M., Corsini, E. M., Pizzella, A., et al. 2000, A&A, 360, 439
Schechter, P. L., & Gunn, J. E. 1978, AJ, 83, 1360
Schulz, H., Knake, A., & Schmidt-Kaler, T. 1994, A&A, 288, 425
Sharples, R. M., Carter, D., Hawarden, T. G., & Longmore, A. J. 1983, MNRAS, 202, 37
Sil'chenko, O. K., Vlasyuk, V. V., & Burenkov, A. N. 1997, A&A, 326, 941
Sofue, Y., & Rubin, V. 2001, ARA&A, 39, 137
Sofue, Y., Tutui, Y., Honma, M., et al. 1999, ApJ, 523, 136
Steiman-Cameron, T. Y., Kormendy, J., & Durisen, R. H. 1992, AJ, 104, 1339
Storchi-Bergmann, T., Redrigues-Ardila, A., Schmitt, H. R., Wilson, A. S., & Baldwin, J. A. 1996, ApJ, 472, 83
van der Kruit, P. C. 1976, A&A, 49,161
van Gorkom, J. H., van der Hulst, J. M., Haschick, A. D., & Tubbs, A. D. 1990, AJ, 99, 1781
Vega Beltran, J. C., Zeilinger, W. W., Amico, P., et al. 1998, A&AS, 131, 105
Veilleux S., Bland-Hawthorn, J., & Cecil, G. 1999, AJ, 118, 2108
Walker, M. F. 1989, PASP, 101, 333
Wilke, K., Möllenhoff, C., & Matthias, M. 1999, A&A, 344, 787
Wilke, K., Möllenhoff, C., & Matthias, M. 2000, A&A, 361, 507
Winge, C., Axon, D. J., Macchetto, F. D., Capetti, A., & Marconi, A. 1999, ApJ, 519, 134
Whitmore, B. C., Lucas, R. A., McElroy, D. B., et al. 1990, AJ, 100, 1489
Zeilinger, W. W, Galletta, G., & Madsen, C. 1990, MNRAS, 246, 324
Zeilinger, W. W., Vega Beltrán, J. C., Rozas, M., et al. 2001, Ap&SS, 276, 643

Online Material

Table 1: Ionized-gas velocity gradients observed along the minor axis of the disk galaxies listed in RSA Catalog.

Object	Morph. Type		D_{25}	i	PA_{MJ}	B_T^0	cz	Class	Obs. PA_{MJ}	Obs. PA_{MN}	References
	[RSA]	[RC3]	[′]	[°]	[°]	[mag]	[km s^{-1}]		[°]	[°]	
(1)	(2)	(3)	(4)	(5)	(6)	(7)	(8)	(9)	(10)	(11)	(12)
S0											
IC 4889	$S0_{1/2}(5)$	E5+	2.9	56	0	11.91	2526	O	0	90	Corsini et al. 2000
NGC 1947	$S0_3(0)$	S0 pec	3.0	32	119	11.50	1157	O	120	30	Mollenhoff 1982
									120	30	Bertola et al. 1992b
NGC 2685	$S0_3(7)$ pec	$(R)SB0^+$ pec	4.5	60	38	11.82	869	G	40	130	Schechter & Gunn. 1978
NGC 3414	$S0_1$	S0 pec	3.5	45	179*	11.86	1434	G	25	115	Lake & Dressler 1986
NGC 3998	$S0_1$	$S0^0(r)$?	2.7	34	140	11.49	1066	C	…	45	Blackman et al. 1983
									140	50	Fisher 1997
NGC 4026	$S0_{1/2}(9)$	S0 sp	5.2	80	178	11.59	930	G	178	88	Fisher 1997
NGC 4111	$S0_1(9)$	$S0^+(r)$: sp	4.6	83	150	11.60	815	G	150	60	Fisher 1997
NGC 4383	S0:	Sa pec?	2.0	60	28	12.38	1663	Z	208	118	Rubin et al. 1999
NGC 4710	$S0_3(9)$	$S0^0(r)$? /	4.9	81	27	11.80	1119	G	27	117	Rubin et al. 1999
NGC 5084	$S0_1(8)$	S0 sp	9.3	88	80	11.28	1706	G	80	170	Zeilinger et al. 1990
NGC 5128	S0+S pec	S0 pec	25.7	40	35	7.30	538	O	35	125	van Gorkom et al. 1990
NGC 5266	$S0_3(5)$ pec (prolate)	$S0^-$:	3.2	50	19	11.50	3074	O	114	15	Caldwell 1984
NGC 5363	$[S0_3(5)]$	I0	4.1	…	135	…	1121	Z	135	45	Sharples et al. 1983
NGC 5866	$S0_3(8)$	$S0^+$ sp	4.7	68	128	10.83	769	Z	128	38	Fisher 1997
NGC 5898	$S0_{2/3}(8)$	E0	2.2	25	37*	11.92	2209	O	66	156	Caon et al. 2000
NGC 7332	$S0_{2/3}(0)$	S0 pec sp	4.1	78	155	11.93	1202	O	155	65	Fisher at al. 1994
S0a/Sa,SB0/Sa,SB0/SBa											
IC 5063	$S0_3(3)$ pec/Sa	$S0^+(s)$:	2.1	49	116	12.58	3408	G	115	25	Danziger et al. 1981
NGC 3489	S03/Sa	SAB0(rs)	3.5	56	70	11.15	690	Z	76	166	Caon et al. 2000
NGC 2787	SB0/a	$SB0^+(r)$	3.2	51	117	11.61	649	O	117	27	Vega Beltràn, priv. comm.
NGC 3941	$SB0_{1/2}/a$	$SB0^0(s)$	3.5	50	10	11.25	934	O	10	100	Fisher 1997
NGC 4036	$S0_3(8)$/Sa	$S0^-$	4.3	69	85	11.49	1397	O	85	175	Fisher 1997
NGC 4546	$SB0_1$/Sa	$SB0^-(s)$:	3.3	66	78	11.25	1014	O	135	45	Bettoni & Galletta 1997
NGC 7049	$S0_3(4)/a$	$S0^0(s)$	4.3	47	57	11.57	2198	C	57	147	Corsini et al. 2003
NGC 7377	$S0_1(3)$/Sa	$S0^+(s)$	3.0	34	101	11.93	3339	O	101	11	Corsini et al. 2003
Sa											
NGC 1316	Sa pec (merger)	$SAB0^0(s)$ pec	12.0	46	50*	9.40	1793	I	50	140	Vega Beltràn, priv. comm.
NGC 2782	Sa(s) pec	SABa(rs) pec	3.5	43	…	12.01	2532	C	90	0	Sakka et al. 1973
								C	75	165	Jogee et al. 1999
NGC 2855	S(r)	(R)S0/a(rs)	2.5	27	130*	12.29	1910	C	120	30	Corsini et al. 2002
NGC 2992	Sa (tides)	Sa pec	3.5	75	15*	12.16	2334	I	17	100	Márquez et al. 1998
NGC 3626	Sa	$(R)S0^+(rs)$	2.7	45	157	11.62	1438	I	157	67	Haynes et al. 2000
NGC 3885	Sa	S0/a(s)	2.4	69	123	12.30	1918	O	123	33	Corsini et al. 2003
NGC 3900	Sa(r)	$S0^+(r)$	3.2	59	2	12.17	1702	C	2	92	Haynes et al. 2000
NGC 4224	Sa	Sa(s): sp	2.6	69	57	12.52	2574	C	57	147	Corsini et al. 2003
NGC 4235	Sa	Sa(s) sp	4.2	82	48	11.89	2343	I	48	138	Corsini et al. 2003
NGC 4424	S(a?) pec	SBa(s) sp	3.6	62	95	11.94	447	G	95	185	Kenney et al. 1996
NGC 4586	Sa	Sa(s): sp	4.0	73	115	12.11	813	C	115	25	Corsini et al. 2003
NGC 4698	Sa	Sab	4.0	53	170	11.24	1032	C	170	80	Sarzi et al. 2000
NGC 4772	Sa:	Sa	3.4	62	147	11.89	1042	C	147	57	Haynes et al. 2000
NGC 4845	Sa	Sab sp	5.0	79	89	11.42	1125	G	78	168	Bertola et al. 1989
NGC 4984	Sa(s)	$(R)SAB0^+(rs)$	2.8	38	90	12.03	1243	O	90	0	Corsini et al. 2003
NGC 5854	Sa	$SB0^+(s)$ sp	2.8	77	55	12.69	1668	Z	55	145	Haynes et al. 2000
NGC 7213	Sa(rs)	Sa(s): sp	3.1	27	124*	11.13	1803	O	124	34	Corsini et al. 2003
SBa											
NGC 2217	SBa(s)	(R)S0	4.5	21	34*	11.35	1609	C	110	20	Bettoni et al. 1990
NGC 3081	SBa(s)	$(R)SAB(r)^0$	2.1	40	158	12.59	2391	O	…	74	Storchi-Bergmann et al. 1996
NGC 7079	SBa	$SB0(s)^0$	2.1	53	82	12.36	2663	G	82	170	Bettoni & Galletta 1997
Sab											
NGC 2460	Sab(s)	Sa(s)	2.5	42	40	12.29	1442	O	40	130	this paper
NGC 4138	Sab(r)	$S0^+(r)$	2.6	50	150	12.10	1039	C	150	60	Jore et al. 1996
NGC 4151	Sab	(R′)SABab(rs):	6.3	46	50	10.71	995*	Z	48	138	Winge et al. 1999
NGC 4388	Sab	Sb(s): sp	5.6	83	92	10.79	2538	I	90	0	Rubin et al. 1999
NGC 4450	Sab pec	Sab(s)	5.2	43	175	10.75	2048	I	175	85	Rubin et al. 1999
NGC 4569	Sab(s)I-II	SABab(rs)	9.6	65	23	9.79	−311	Z	23.5	113.5	Rubin et al. 1999
NGC 4579	Sab(s)II	SABb(rs)	5.9	38	95	10.29	1627	O	275	185	Rubin et al. 1999
NGC 4826	Sab(s)II	(R)Sab(rs)	10.0	59	115	8.82	474	Z	115	25	Rubin 1994
NGC 7177	Sab(r)II.2	SABab(r)	3.1	51	90	11.47	1112	Z	90	0	Márquez et al. 2002
SBab											

Tab. 1: (continue).

NGC 4419	SBab:	SBa(s)	3.3	74	133	11.60	−224	O	133	43	Rubin et al. 1999
Sb											
NGC 224	SbI-II	Sb(s)	190.5	72	35	3.36	−295	I	…	128	Sandqvist et al. 1989
									38	128	Pellet 1976
									38	128	Rubin & Ford 1970
NGC 891	Sb on edge	Sb(s)? sp	13.5	81	22	9.37	528*	Z	22	112	Keppel et al. 1991
NGC 1961	Sb(rs)II pec	SABc(rs)	4.6	50	85	11.01	3983	Z	85	175	Rubin et al. 1979
NGC 2841	Sb	Sb(r)	8.1	64	147	9.58	635	G	150	62	Sil'chenko et al. 1997
NGC 3031	Sb(r)I-II	Sab(s)	26.9	59	157	7.39	−49	G	150	60	Goad 1974
NGC 3504	Sb(s)/SBb(s)I-II	(R)SABab(s)	2.7	39	57*	11.65	1518	Z	152	62	Burbidge, et al. 1960
NGC 3521	Sb(s)II-III	SABbc(rs)	11.0	63	163	9.29	782	Z	163	73	Zeilinger et al. 2001
NGC 4192	SBII:	SABb(s)	9.8	75	155	10.02	−126	I	155	65	Rubin et al. 1999
NGC 4258	Sb(s)II	SABbc(s)	18.6	68	150	8.53	480	G	148	58	Chincarini & Walker 1967
									150	…	Sofue et al. 1999
NGC 4527	RSb(rs)II	SABbc(s)	6.2	71	67	10.66	1727	I	67	157	Rubin et al. 1999
NGC 5172	SbI	SABbc(rs):	3.3	59	103	12.10	4337	Z	103	13	Márquez et al. 2002
NGC 6810	Sb	Sab(s):sp	3.3	78	176	11.49	1958	I	176	86	this paper
NGC 6951	Sb/SBb(rs)I.3	SABbc(rs)	3.9	34	170	10.71	1331	I	138	48	Perez et al. 2000
NGC 7217	Sb(r)II-III	(R)Sab(r)	3.9	34	95	10.53	935	G	86	10	Peterson et al. 1978
NGC 7331	Sb(rs)I-II	Sb(s)	10.5	70	171	9.38	835	Z	171	77	Rubin et al. 1965
SBb											
NGC 1300	SBb(s)I.2	SBbc(rs)	6.2	49	106	10.77	1592	C	103	185	Peterson et al. 1980
NGC 1365	SBb(s)I	SBb(s)	11.2	57	32	9.93	1675	G	225	318	Lindblad et al. 1996
NGC 3992	SBb(rs)I	SBbc(rs)	7.6	52	68	10.26	1059	O	67	152	Wilke et al. 2000
NGC 4639	SBb(r)II	SABbc(rs)	2.8	48	123	11.85	898	C	124	34	Rubin et al. 1999
NGC 5728	SBb(rs)II	SABa(r):	3.1	55	30	11.65	2885	C	33	123	Rubin et al. 1980
NGC 5850	SBb(sr)I-II	SBb(r)	4.3	30	140	11.39	2483	Z	163	73	Higdon et al. 1980
NGC 6300	SBb(s)II pec	SBb(rs)	4.5	49	118	10.20	1064	C	111	21	Buta 1987
NGC 6951	Sb/SBb(rs)I.3	SABbc(rs)	3.9	34	170	10.71	1331	I	138	48	Perez et al. 2000
Sbc											
NGC 3310	Sbc(r) pec	SABbc(r) pec	3.1	40	…	10.95	1018	I	150	60	Mulder & van Driel 1996
NGC 4433	SbcIII	SABab(s)	2.2	65	5	12.64	2942	G	0	90	Chromey 1974
NGC 4501	Sbc(s)II	Sb(rs)	6.9	59	140	9.86	2120	Z	320	210	Rubin et al. 1999
NGC 4580	Sbc(r)II	SABs(rs) pec	2.1	40	165	12.49	1227	G	345	255	Rubin et al. 1999
NGC 5194	Sbc(s)I-II	SAbc(s) pec	11.2	53	163	8.67	463	I	170	80	Kuno et al. 1997
NGC 5248	Sbc(s)I-II	SABbc(rs)	6.2	44	110	10.63	1189	Z	113	23	Burbidge et al. 1962
NGC 6221	Sbc(s)II-III	SBc(s)	3.5	47	5	9.77	1350	I	5	95	Vega Beltràn et al. 1998
NGC 6574	Sbc(r)II	SABbc(rs):	1.4	40	160	11.79	2321	C	159	66	Demoulin 1969
NGC 6814	Sbc(rs)I-II	SABbc(rs)	3.0	21	89*	11.32	1509	Z	90	0	Schulz et al. 1994
SBbc											
NGC 2336	SBbc(r)I	SABbc(r)	7.1	58	178	10.61	2205	C	5	94	Wilke et al. 1999
NGC 7479	SBbc(s)I-II	SBc(s)	4.1	41	25	11.22	2394	I	35	125	Wilke et al. 2000
Sc											
NGC 157	Sc(s)II-III	SABbc(rs)	4.2	50	30	10.59	1730	Z	…	130	Ryder et al. 1998
									224	…	Fridman et al. 2001
NGC 253	Sc(s)	SABc(s)	27.5	77	52	7.09	240	I	52	321	Prada et al. 1998
NGC 949	Sc(s)III	Sb(rs):?	2.4	58	145	11.78	596	I	145	55	this paper
NGC 1084	Sc(s)II.2	Sc(s)	3.2	56	35	10.90	1414	Z	33	123	Burbidge et al. 1963
NGC 1087	Sc(s)III.3	SABc(rs)	3.7	53	5	10.97	1508	Z	0	90	Blackman 1980a
NGC 1792	Sc(s)II	SAbc(rs)	5.2	61	137	10.36	1218	Z	140	50	Rubin et al. 1964
NGC 2541	Sc(s)III	Scd(s)	6.3	60	165	11.57	628	C	165	75	this paper
NGC 2748	Sc(s)II-III	SAbc	3.0	68	38	11.59	1456	G	44	134	Reshetnikov & Combes 1994
NGC 2776	Sc(s)I	SABc(rs)	3.0	27	93*	11.96	2618	G	90	0	Carozzi 1979
NGC 2903	ScIII pec	SABbc(rs)	12.6	62	17	9.11	565	O	9	103	Walker 1989
NGC 2998	Sc(s)II	SABc(rs)	2.9	63	53	12.52	4767	Z	53	143	Rubin et al. 1980
NGC 3079	Sc pec	SBc(s) sp	7.9	81	165	10.41	1101	Z	169	79	Veilleux et al. 1999
NGC 3495	Sc(s)III	Sd:	4.9	77	20	10.74	1086	Z	20	110	Rubin et al. 1980
NGC 3672	Sc(s)I-II	Sc(s)	4.2	63	12	11.41	1857	C	8	98	Rubin et al. 1977
NGC 3684	Sc(s)II	Sbc(rs)	3.1	47	130	11.82	1394	Z	128	38	Blackman 1980b
NGC 4100	Sc(s)I-II	(R′)Sbc(rs)	5.4	72	167	11.05	1131	G	…	78	Afanaz'ev et al. 1992
NGC 4212	Sc(s)II-III	Sc:	3.2	52	75	11.35	377	Z	75	165	Rubin et al. 1999
NGC 4237	Sc(r)II.8	SABbc(rs)	2.1	50	108	12.18	865	Z	108	18	Rubin et al. 1999
NGC 4298	Sc(s)III	Sc(rs)	3.2	56	140	11.62	1122	I	140	50	Rubin et al. 1999
NGC 4303	Sc(s)I.2	SABbc(rs)	6.5	27	162*	10.12	1607	I	318	228	Rubin et al. 1999
NGC 4321	Sc(s)I	SABbc(s)	7.4	32	30	9.98	1579	O	350	260	Rubin et al. 1999
NGC 4420	Sc(s)III	SBbc(r):	2.0	62	8	12.28	1711	Z	8	98	Rubin et al. 1999
NGC 4536	Sc(s)I	SABbc(rs)	7.6	65	130	10.58	1894	Z	…	40	Afanaz'ev et al. 1992
NGC 4567	Sc(s)II-III	Sbc(rs)	3.0	48	85	11.79	2213	I	85	175	Rubin et al. 1999

Tab. 1: (continue).

NGC 4568	Sc(s)II-III	Sbc(rs)	4.6	65	23	11.18	2260	Z	23	113	Rubin et al. 1999
NGC 4571	Sc(s)II-III	Sd(r)	3.6	27	55	11.73	284	Z	40	130	Rubin et al. 1999
NGC 4595	Sc(s)II.8	SABb(rs)?	1.7	50	110	12.62	589	Z	110	200	Rubin et al. 1999
NGC 4647	Sc(s)III	SABc(rs)	2.9	38	125	11.81	1421	O	124	214	Rubin et al. 1999
NGC 4651	Sc(r)I-II	Sc(rs)	4.0	49	80	11.04	788	C	71	161	Rubin et al. 1999
NGC 4808	Sc(s)III	Scd(s):	2.8	66	127	11.82	738	Z	127	37	Rubin et al. 1999
NGC 4945	Sc	SBcd(s): sp	20.0	81	43	7.43	581	G	42	132	Peterson 1980
NGC 5012	Sc(rs)I-II	SABc(rs)	2.9	55	10	12.49	2661	Z	10	170	Márquez et al. 2002
NGC 5457	Sc(s)I	SABcd(rs)	28.8	21	…	8.21	221	Z	35	125	Comte et al. 1979
NGC 5480	Sc(s)III	Sc(s):	1.7	49	0	12.49	1823	I	177	87	Márquez et al. 2002
NGC 5962	Sc(r)II.3	Sc(r)	3.0	45	110	11.73	1993	C	110	20	Márquez & Moles 1996
NGC 6070	Sc(s)I	Scd(s)	3.5	59	62	11.58	2007	I	62	152	Márquez et al. 2002
NGC 6106	Sc(rs)II.3	Sc	2.5	57	140	12.22	1464	Z	140	50	Márquez et al. 2002
NGC 6946	Sc(s)II	SABcd(rs)	11.5	32	…	7.78	7	O	67	157	Munoz Tunon et al. 1987
NGC 7541	Sc(s)II	SBbc(rs): pec	3.5	70	102	11.57	2669	Z	…	15	Kyazumov 1980
SBc											
NGC 4064	SBc(s):	SBa(s): pec	4.4	67	150	11.75	1000	G	150	60	Rubin et al. 1999
NGC 4178	SBc(s)II	SBdm(rs)	5.1	70	30	11.35	240	Z	30	120	Rubin et al. 1999
NGC 4294	SBc(s)II-III	SBcd(s)	3.2	68	155	11.83	421	Z	155	65	Rubin et al. 1999
NGC 4535	SBc(s)I.3	SABc(s)	7.1	45	0	10.32	1973	C	0	90	Rubin et al. 1999
NGC 4654	SBc(rs)II	SABcd(rs)	4.9	55	128	10.75	1035	Z	128	38	Rubin et al. 1999
NGC 4713	Sbc(s)II-III	SABd(rs)	2.7	51	100	11.85	631	Z	100	10	Rubin et al. 1999
NGC 7070	SBc(s)II.8	Scd(s)	2.3	39	23*	12.55	2369*	Z	29	119	Sharples at al. 1983
Scd											
NGC 4490	Scd III pec	SBd(s) pec	6.3	61	125	9.81	594	I	125	62	Duval 1981
Sm, Im											
NGC 1156	SmIV	IBm(s)	3.3	42	25	11.41	372	C	25	115	Hunter et al. 2002
NGC 2366	SBmIV-V	IBm(s)	8.1	66	25	10.95	87	I	30	120	Hunter et al. 2002
NGC 4449	SmIV	IBm	6.2	45	45	9.94	211	Z	45	135	Hunter et al. 2002
S											
NGC 1487	S pec tides	pec	3.3	50	55	11.92*	733	G	…	160	Aguero & Paolantonio 1997
NGC 3691	S	SBb?	1.3	42	15	12.95	997	Z	191	100	Blackman 1980b
NGC 3955	S pec	S0/a pec	2.9	74	165	12.03	1515	G	166	76	Chromery 1974
SB											
NGC 4670	SB pec	SB^0(s): pec	1.4	41	90	12.89	1112	Z	90	0	Sakka et al. 1973

NOTES – Data are taken from RC3 except for those marked with *, which are taken from LEDA. Col.(2): morphological classification from RSA. Col.(3): morphological classification from RC3. Col.(4): major-axis isophotal diameter measured at the surface brightness level μ_B = 25.0 mag arcsec^{-2} from RC3. Col.(5): inclination derived as $\cos^2 i = (q^2 - q_0^2)/(1 - q_0^2)$. The observed axial ratio q is taken from RC3 and the intrinsic flattening has been assumed following Guthrie (1992) with RC3 morphological classification. Col.(6): major-axis position angle from RC3. Col.(7): apparent total blue magnitude corrected for inclination, extinction and redshift from RC3. Col.(8): optical recession velocity from RC3. Col.(9): classification of the minor-axis **velocity profiles** as described in Sect.2. Col.(10): observed position angle which is closest to the galaxy major axis. Col.(11): observed position angle which is closest to the galaxy minor axis. Col.(12): reference for gas kinematics measured along the observed position angles.